Mechanics of Materials 175 (2022) 104478

Contents lists available at ScienceDirect

Mechanics of Materials

journal homepage: www.elsevier.com/locate/mechmat

Off-axis tensile performance of notched resin-infused thermoplastic 3D fibre-reinforced composites

S.Z.H. Shah [a], P.S.M. Megat-Yusoff [a], Tahir Sharif [b], Syed Zahid Hussain [c], R.S. Choudhry [b,*]

[a] Department of Mechanical Engineering, Universiti Teknologi PETRONAS,32610 Bandar Seri Iskandar, Perak, Malaysia
[b] College of Science and Engineering, School of Computing and Engineering, Mechanical Engineering Discipline, University of Derby, UK
[c] Department of Mechatronics Engineering, Air University E-9 Islamabad, Pakistan

ARTICLE INFO

Keywords:
3-Dimensional reinforcement
Thermoplastic resin (elium)
Notched tension
Digital image correlation

ABSTRACT

This study presents a comparison of off-axis tensile performance for notched (open-hole) and unnotched (no-hole) 3D fibre reinforced composites (FRC) specimens having two different types of matrices. The two matrix systems compared are, a novel infusible thermoplastic (Elium) resin and conventional thermoset (epoxy). Three different configurations, (one unnotched and two notched) were tested for each 3D-FRC. The resulting notched net strength, gross strength, failure strains, notch sensitivity and energy absorbed by each configuration were evaluated and compared. Additionally, 2D digital image correlation (DIC) was used to evaluate full-field strain distribution in each case. The results elucidate that thermoplastic 3D-FRCs are notch insensitive irrespective of the notch size and possess higher failure strains (around 30 percent in the cases investigated) and energy absorption (around 33 percent in the cases investigated). In contrast, thermoset 3D-FRC appeared to be notch sensitive, as the notched size increased, and they failed at lower axial strains (up to 60 percent reduction compared to unnotched specimens for the size investigated). Thus, resin-infused thermoplastic off-axis configurations are effective for composite joint applications, particularly in notch-insensitive designs, requiring higher energy absorption and failure strains.

Author statement

Syed Zulfiqar Hussain Shah: Conceptualization, Methodology, Formal analysis, Investigation, Visualization, Writing - Original Draft, Funding acquisition, Puteri Sri Melor Megat-Yusoff: Supervision, Investigation, Project administration, Rizwan Saeed Choudhry: Supervision, Methodology, Investigation, Writing - Original Draft, Writing-Reviewing and Editing, Tahir Sharif: Investigation, Writing- Reviewing and Editing, Syed Zahid Hussain: Resources.

1. Introduction

Three-dimensional (3D) woven composites are gaining popularity in structural applications, due to their superior through-thickness properties, excellent impact resistance, damage tolerance and ability to produce near-net-shape designs, in comparison with laminated composites (Shah et al., 2017, 2019, 2022). Complex-shaped composite structures are made by joining simpler composite parts through different techniques such as adhesive bonding, mechanically fastening and hybrid joining (combined bolted and bonded joints) (Sajid et al., 2021a, 2021b, 2022). This requires drilling holes or notches for assembly and mechanical fastening, resulting in geometric discontinuities and stress-concentration around the holes, which potentially degrades the strength and long-term performance of composite parts (Guo et al., 2021). Thus, investigating the notched strength and failure mechanisms of FRC is critical for the safety of the composite structure. The efficient joint design requires a material with higher ductility (to distribute stress around holes), notch insensitivity (ultimate strength/strain are insensitive to notch), failure strain and energy absorption (Saleh et al., 2016).

Several authors studied the notched response of 2D-FRC (unidirectional and woven composites). It was observed that the notched strength of woven composites is less sensitive as compared to the unidirectional composites, due to their better resistance against delamination and crack propagation (Mohammadi et al., 2017; Awerbuch and Madhukar, 1985; Yudhanto et al., 2012). Nevertheless, limited literature has been reported on the characterization of the notched response of 3D-FRC. The presence of through-thickness reinforcement increases the fracture toughness of FRC, which further reduces their notched sensitivity and

* Corresponding author.
E-mail address: r.choudhry@derby.ac.uk (R.S. Choudhry).

https://doi.org/10.1016/j.mechmat.2022.104478
Received 19 May 2022; Received in revised form 17 September 2022; Accepted 18 September 2022
Available online 27 September 2022

improves their notched strength compared to 2D-FRC. Dai et al. (2015) studied the on-axis notched strength of carbon/epoxy 3D-FRC using two different sizes (i.e., diameter to width ratio of 0.164 and 0.5). The maximum reduction in the notched strength reported was 17% compared to the unnotched strength. Saleh et al. (2016) investigated the notched response of off-axis carbon/epoxy 3D-FRC using a diameter-to-width ratio of 0.166 and found up to a 10% reduction in the notched strength. Song et al. (2019) studied the effect of temperature on the notched performance of carbon-epoxy 3D-FRC. The authors concluded that at elevated temperature notched strength decreased by 26% compared to room temperature. Recently, Guo et al. (2021) studied the effect of different notches on carbon/epoxy 3D-FRC. The authors found that the notched strength was reduced by 35% compared to unnotched composites. All these studies were focused on the thermoset (carbon-epoxy) based 3D-FRC, which exhibits lower ductility and failure strain. However, no study has been dedicated to evaluating the notched behaviour/sensitivity of newer resin-infused thermoplastic 3D-FRC.

Recently, a company named Arkema developed liquid thermoplastic resin (Elium), to fabricate rein-infused thermoplastic composites using a conventional vacuum infusion process. The resin-infused thermoplastic 3D-FRC showed excellent impact resistance (Shah et al., 2020, 2021a), damage tolerance (Shah et al., 2021b), and quasi-static crush performance (Shah et al., 2021c); however, to the best of the author's knowledge unnotched and notched performance of resin-infused thermoplastic composites, particularly resin-infused thermoplastic 3D-FRC and their comparison with thermoset 3D-FRC is not available in the open literature. This suggests that the notched tension performance of off-axis resin-infused thermoplastic 3D-FRC is not completely understood, thus there is a strong need to investigate these properties for their growing application in composite structures. With this aim, the specific objectives of this work are to (a) evaluate the notched tension performance of off-axis resin-infused thermoplastic 3D-FRC under quasi-static tensile load, (b) determine notch sensitivity and energy absorption of resin-infused thermoplastic 3D-FRC, (c) evaluate strain-fields distribution using digital image corelation (DIC), and (d) to benchmark their performance compare the results with conventional off-axis thermoset (epoxy) 3D-FRC. This work makes an important contribution in understanding the notched tension behaviour and failure mechanisms of novel resin-infused thermoplastic 3D-FRC. This information is of great significance in the design of composites joints for structural applications of these composites.

2. Materials and methods

2.1. Materials

This study uses 3D orthogonal E-glass woven fabric obtained from TexTech® Industries, United States. The fabric has an overall thickness of 4.3 mm and an areal density of 5200 GSM. The acrylic thermoplastic liquid resin Elium® 188 × 0 from Arkema and the thermoset epoxy resin system Epolam® 5015/5015 from Axson are utilized for the fabrication of thermoplastic and thermoset 3D-FRC specimens. The elastic constants and properties of both resin systems are summarised in Table 1.

A vacuum-assisted resin infusion process was used to fabricate both 3D-FRC specimens. The fabricated specimens have a total thickness of 4 mm ± 0.1 mm. Further information about the fabrication process of thermoplastic and thermoset 3D-FRC can be found in our previous publication (Shah et al., 2020). The properties of fabricated thermoplastic and thermoset 3D-FRC panels are summarised in Table 2.

2.2. Test method

The off-axis notched and unnotched tensile tests were performed on both thermoplastic and thermoset 3D-FRC, according to ASTM standards D5766 (ASTM D5766/D5766M-11(2018), 2018) and D3039 (ASTM, 2017), respectively. Table 3 shows a total of 6 configurations determined based on the thermoplastic (unnotched (TP Case-A) and notched (TP Case-B and TP Case-C)) and thermoset (unnotched (TS Case-A) and notched (TS Case-B and TS Case-C)) 3D-FRC. The ASTM standard D5766 is used to measure the notched tensile (OHT) strength of polymer composites, the recommended specimen size is 200 × 36 mm^2 with a 6 mm hole diameter (diameter to width ratio is 0.166). In this study, the samples were carefully cut using a water-based diamond tip disc cutter and the holes were drilled using a silicon carbide drill bit to minimise damage. After the cutting and drilling operation, the integrity of the samples was physically checked under a microscope.

The study's goal is to evaluate the notched strength of off-axis thermoplastic and thermoset 3D-FRC specimens to that of unnotched specimens. Therefore, notched and unnotched specimens were cut with the same dimensions, i.e., 250 × 25 mm^2. In Case-B, a 4.1 mm diameter hole was drilled to maintain the same diameter to width ratio (0.166), as recommended by the standard, whereas, for Case-C a large, notched size of 10 mm was used which has a diameter to width ratio (0.4), see Fig. 1

Table 1
Properties of elium 188×0 and Epolam5015/5015.

Material Properties	Elium®	Epolam® 5015
Modulus of Elasticity (GPa)[c]	3.1	3.3
Modulus of Rigidity (GPa)[c]	1.31	1.15
Poisson's Ratio[c]	0.37	0.3
Viscosity (mPa.s)	200	210
Elongation at failure (%)[a]	6	3.5
Fracture toughness (kJ/m^2)[b]	0.5	0.12
Rockwell Hardness[d]	99	119

[a] Reported in literature (Elium®. 188 × 0 (Kazemi et al., 2019) and Epolam®. 5015/5015 (Zhang and Yang, 2014)).
[b] Reported in literature (Bhudolia et al., 2017).
[C] Reported in literature (Shah et al., 2021a).
[d] In-house testing.

Table 2
Physical parameters of the cured panel (average of ten samples).

Parameters	3D thermoplastic FRC	3D thermoset FRC
Thickness (mm)	4 ± 0.1	4 ± 0.1
Fiber volume fraction (%)	52 ± 1.5	52 ± 0.4
Void content (%)	2.7 ± 1	<1 ± 0.3
Density (g/cc)	1.86 ± 0.02	1.92 ± 0.01

Table 3
Different off-axis configurations of thermoplastic (TP) and thermoset (TS) 3D-FRC.

Details	No of repeats	**Hole diameter (mm)**	**Dimensions l (mm) × w (mm)**	Intact area A_i **(mm^2)**	**Hole dia. to width ratio d_r**
TP Case-A	3	–	250 × 25	100	1
TP Case-B	3	4.1	250 × 25	83.6	0.164
TP Case-C	3	10	250 × 25	60	0.4
TS Case-A	3	–	250 × 25	100	1
TS Case-B	3	4.1	250 × 25	83.6	0.164
TS Case-C	3	10	250 × 25	60	0.4

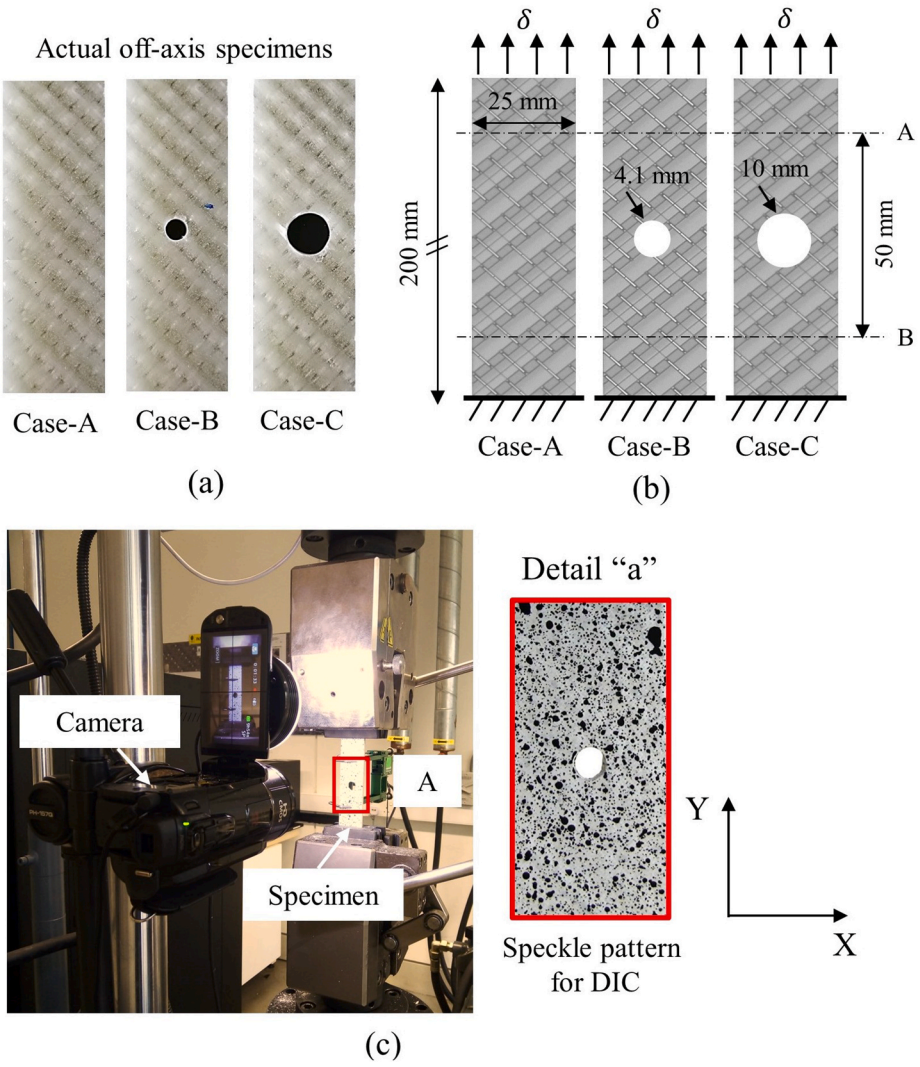

Fig. 1. Testing configurations and setup. (a) actual machined samples, (b) schematic diagram of specimens along with their dimensions and boundary conditions, and (c) testing setup along with DIC setup.

(a). Three repeats were performed for each experiment.

These tests were conducted on ZwickRoell hydraulic-driven load frame, equipped with a 50 kN load cell to record the force experienced by the specimen at each time step. The schematic diagram of boundary conditions is shown in Fig. 1(b). A displacement-controlled load rate of 2 mm/min was applied, and the resulting strains were measured using strain gauges and digital image correlation (DIC). In this study, 2D DIC was used to measure strain fields in the gauge section of the specimen, whereas 350 Ohm's KFRPB series (KYOWA) strain gauges (5 mm grid length) were utilized to validate DIC strain measurement. The coupon's surface was prepared for DIC measurement by first spraying it with flat white paint, followed by random speckles with flat black paint, as shown in Fig. 1(c). A single Cannon Legria® 8-megapixel digital camera was used to capture the video, which is then post-processed using GOM® correlate software to evaluate strain fields.

2.3. Evaluation method

The unnotched and open-hole performance is compared based on several parameters. These include global load P vs. deflection δ response obtained from load frame, net axial tensile strength σ_{yy}^{net}, net shear strength σ_{xy}^{net}, gross axial tensile strength σ_{yy}^{gross}, gross shear strength σ_{xy}^{gross}, net-SCF K_{tn}, gross-SCF K_{tg}, localized strain field, maximum tensile strain ε_{max} obtained from DIC, energy absorption E_{abs} and notched sensitivity. The net axial tensile strength and net shear strength are evaluated using applied load P and net cross-sectional area A_n, given by Eqns. (1) and (2).

$$\sigma_{yy}^{net} = \frac{P}{A_n} = \frac{P}{t(w-d)} \tag{1}$$

$$\sigma_{xy}^{net} = \pm \frac{\sigma_{yy}^{net}}{2} \tag{2}$$

The gross axial tensile strength and gross shear strength are calculated using applied load and gross cross-sectional area A_g (Hodgkinson, 2012), using Eqns. (3) and (4).

$$\sigma_{yy}^{gross} = \frac{P}{A_g} = \frac{P}{tw} \tag{3}$$

$$\sigma_{xy}^{gross} = \pm \frac{\sigma_{yy}^{gross}}{2} \tag{4}$$

The localized strains were measured using DIC between lines A-B; 50 mm apart as highlighted in Fig. 1(b). The energy absorbed in each case is established from the load-deflection curves up to the complete failure, i.e., $E_{abs} = \int_0^{\delta} F(\delta)d\delta$.

In this study, net-SCF K_{tn} and gross-SCF K_{tg} factors were used to evaluate theoretical loads for failure initiation for Case-B and Case-C. The SCF was evaluated based on the analytical formulation proposed by Lekhnitskii (Russo and Zuccarello, 2007) and Tan (1988) for composite laminate members (CLM). Lekhnitskii (Russo and Zuccarello, 2007) presented an analytical formulation to evaluate gross-SCF K_{tg}^{∞} of an infinite thin unidirectional homogenous CLM with a central circular hole, given by Eqn. (5).

$$K_{tg}^{\infty} = 1 + \sqrt{2\left(\sqrt{\frac{E_x}{E_y}} - \nu_{xy}\right) + \frac{E_x}{G_{xy}}} \tag{5}$$

where, E_x, E_y, ν_{xy} and G_{xy} represent longitudinal modulus, transverse modulus, Poisson's ratio, and shear modulus. The material properties used to evaluate gross-SCF K_{tg}^{∞} are given in Table 4. There is no exact formulation for calculating the SCF for a finite thin composite laminate member. Tan (1988) proposed an approximate solution to determine the SCF ratio based on the finite-width correction factor M, given by Eqn. (6).

$$SCF\ Ratio = \frac{K_{tg}^{\infty}}{K_{tg}} = \frac{3(1-d_r)}{2+(1-d_r)^3} + \frac{1}{2}(d_r M)^6\left(K_{tg}^{\infty} - 3\right)\left[1-(d_r M)^2\right] \tag{6}$$

$$M^2 = \frac{\sqrt{1 - 8\left[\frac{3(1-d_r)}{2+(1-d_r)^3} - 1\right]} - 1}{2d_r{}^2}$$

where K_{tg} represents gross-SCF of CLM finite width. The net-SCF K_{tn} is then determined using gross-SCF K_{tg} factors, net cross-sectional area A_n and gross cross-sectional area A_g, given by Eqn. (7).

$$K_{tn} = K_{tg}\frac{(A_g - dt)}{A_g} \tag{7}$$

$$\frac{K_{tg}}{K_{tn}} = \frac{\sigma_n}{\sigma_g} = \frac{A_n}{A_g}$$

The net-SCF and gross-SCF are then used to evaluate theoretical failure initiation load, $F_{n/g}^{ini}$ for off-axis 3D-FRC, using Eqn. (8).

$$F_{n/g}^{ini} = \frac{\sigma_{yy}^{gross} A^{net}}{SCF_{n/g}^{AP}} \tag{8}$$

where, $SCF_{n/g}^{AP}$, represent net/gross-SCF of angle-ply, which is evaluated using net/gross-SCF of UD-ply $SCF_{n/g}^{UD}$ and correction factor c_f for angle ply laminates due to orientation and averaging effect, i.e., $SCF_{n/g}^{AP} = SCF_{n/g}^{UD}/c_f$. The correction factor is determined based on the FE analysis reported in (Ahmed et al., 2015). The correction factor for Case-B and Case-C are 2.2 and 2.5, respectively.

The notch sensitivity is determined using normalized strength σ_{nn}^{gross} vs. hole diameter to width ratio $d_r = d/w$ (Muñoz et al., 2014), where normalized strength is a ratio between axial gross strength and axial net strength, i.e., $\sigma_{nn}^{gross} = \sigma_{yy}^{gross}/\sigma_{yy}^{net}$. Thus, in order to evaluate the notch sensitivity of off-axis 3D-FRC at a specific hole diameter to width ratio, notched axial ultimate tensile strength measured experimentally is normalized with un-notched axial ultimate tensile strength measured experimentally. The normalized value is then compared to the ideal ductile "notch insensitive" and ideal brittle "notch sensitive" curves. The ideal notch insensitive response of a ductile material is given by Eqn. (9) and ideal notch sensitive response of brittle material is given by Eqn. (10) (Saleh et al., 2016).

$$\frac{\sigma_{yy}^{net}}{\sigma_{yy}^{gross}} = 1 - \left(\frac{D}{W}\right) \tag{9}$$

$$\frac{\sigma_{yy}^{net}}{\sigma_{yy}^{gross}} = \left[1 - \left(\frac{D}{W}\right)\right] \Big/ K_T \tag{10}$$

$$K_T = 2 + [1 - (D/W)]^3$$

In many applications failure initiation load is the key design parameter thus, we have also evaluated performance (notch sensitivity) by comparing the theoretical failure initiation load in each case with the actual (experimental) failure initiation load determined from the point where the stress, strain curve starts to become non-linear.

Table 4
Material properties used to evaluate SCF.

Property	3D-TP-FRC	3D-TS-FRC
E_{11} (GPa)	27.1	33.4
E_{22} (GPa)	26.4	31.0
ν_{12}	0.08	0.12
G_{12} (GPa)	4.3	4.5

3. Results and discussion

3.1. Comparison of load/displacement curves

The load/displacement curves of off-axis unnotched (Case-A) and notched (Case-B and Case-C) resin-infused thermoplastic and thermoset 3D-FRCs are shown in Fig. 2. Both notched and unnotched 3D-FRC exhibit an initial linear response, which is followed by the significant nonlinear shear (NLS) region. The transition load from the linear-to-nonlinear region in thermoplastic and thermoset 3 F-FRC is ~4 kN and ~5.5 kN, respectively. This lower transitional load in thermoplastic 3D-FRC is attributed to early nonlinear shear deformation caused by lower stiffness and higher ductility of the thermoplastic matrix. The final failure in all the cases is characterised by a sudden load drop, after reaching peak load values. However, prior to this peak load, the thermoplastic 3D-FRC exhibits greater non-linear shear behaviour, and the final failure occurs at a higher displacement than the thermoset counterpart (Case-A and Case-B, in Fig. 2(b)). In unnotched specimens both 3D-FRC showed almost similar failure load (Case-A in Fig. 2(a)–b), in contrast among notched specimens, the thermoset 3D-FRC depicts lower failure load and displacement, compared to thermoplastic 3D-FRC (Case-B and Case-C in Fig. 2(a)). The final failure state in each case is shown in Fig. 2(c)–d. The thermoplastic 3D-FRC shows higher displacement at complete failure, due to higher fracture toughness of thermoplastic resin and stronger interface which is indicated by the localized debonding upon significant plastic scissoring (see Fig. 2(c)). In contrast, thermoset 3D-FRC shows significant fibre pullout and debonding (see Fig. 2(d)). The ultimate load, gross tensile strength, net tensile strength, localized failure strains and energy absorbed up to the complete failure in each case along with the deviation among three samples, are given in Table 5.

In the case of gross axial tensile strength, the notched thermoplastic 3D-FRC shows 15.9% (Case-B) and 43% (Case-C) reduction, whereas thermoset 3D-FRC shows 20% (Case-B) and 50% (Case-C) reduction, in comparison with unnotched specimens (see Fig. 3(a)). In addition, the thermoset 3D-FRC shows up to a 20% reduction in the net axial strength (Case-C), compared to 5% in thermoplastic 3D-FRC (Case-C). In the case of localized failure strains, notched thermoplastic 3D-FRC depicts 2% (Case-B) and 32% (Case-C) reduction, in contrast, notched thermoset 3D-FRC shows 33% (Case-B) and 60% (Case-C) reduction compared to unnotched specimens (see Fig. 3(c)). For energy absorbed by both 3D-FRC, notched specimens show a significant reduction in the absorbed energy as the notched size increases, i.e., up to 90% compared to unnotched specimens. Among Case-B and Case-C, the thermoplastic 3D-FRC shows 32.2% and 33% higher energy absorption relative to thermoset specimens respectively, (see Fig. 3(d)).

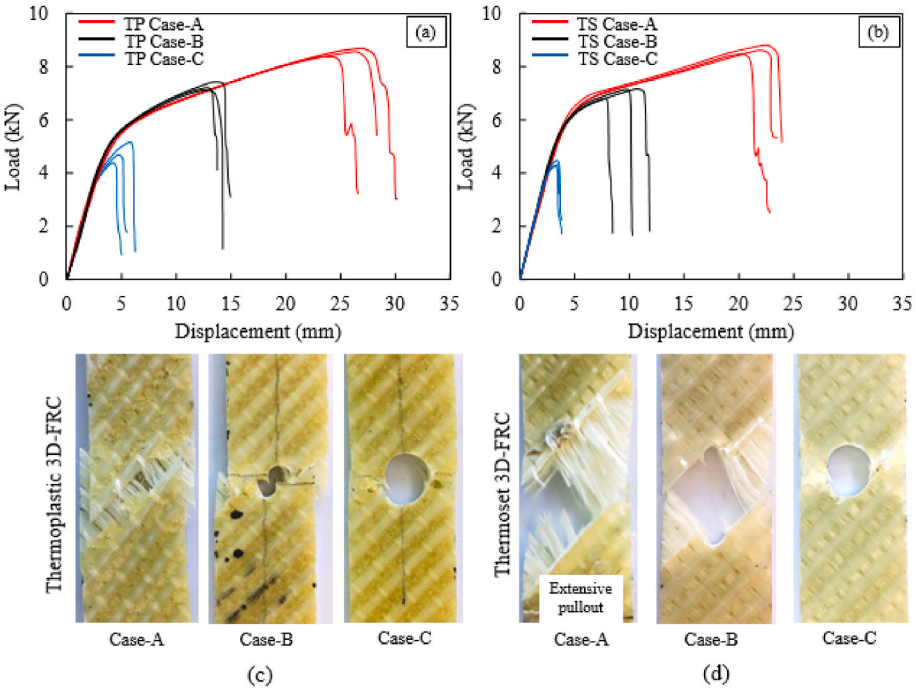

Fig. 2. Comparison of load/displacement curves of the notched and unnotched 3D-FRC. (a) Thermoplastic 3D-FRC, (b) thermoset 3D-FRC, (c) final damage state of thermoplastic 3D-FRC and (d) final damage state of thermoset 3D-FRC.

Table 5
Summary of results obtained from unnotched and notched tensile tests.

Configurations/Property	TP Case-A	TP Case-B	TP Case-C	TS Case-A	TS Case-B	TS Case-C
F_{max} (kN)	8.54 (±0.12)	7.18 (±0.16)	4.87 (±0.22)	8.61 (±0.1)	6.93 (±0.2)	4.31 (±0.15)
σ_{yy}^{gross} (MPa)	85.4 (±1.2)	71.8 (±1.6)	48.7 (±2.2)	86.1 (±1)	69.3 (±2.0)	43.1 (±1.5)
σ_{yy}^{net} (MPa)	85.4 (±1.2)	85.8 (±1.6)	81.2 (±2.2)	86.1 (±1)	82.9 (±2.0)	71.8 (±1.5)
σ_{xy}^{gross} (MPa)	42.6 (±1.2)	35.9 (±1.6)	24.35 (±2.2)	43.1 (±1)	34.6 (±2.0)	21.6 (±1.5)
σ_{xy}^{net} (MPa)	42.7 (±1.2)	42.9 (±1.6)	40.6 (±2.2)	43.0 (±1)	41.4 (±2.0)	35.9 (±1.5)
ε_{max} (%)	10.2 (±0.8)	10.0 (±0.4)	6.9 (±0.5)	9.9 (±0.7)	6.6 (±0.9)	4.0 (±0.5)
E_{abs} (MJ.m^{-3})	186.1 (±15.3)	77.0 (±4.25)	17.0 (±3.8)	156.7 (±10.5)	52.2 (±11.5)	10.6 (±0.8)

To evaluate the notch sensitivity of off-axis thermoplastic and thermoset 3D-FRC, the gross tensile strength is normalized with net strength and plotted against the hole-diameter to specimen width ratio, see Fig. 3 (e). The normalized strength is close to the straight dotted line, this suggests that the gross strength is proportional to net strength (particularly for 0.164 diameter-to-width ratios), given by equation (9). As a result, the stress concentration caused by the circular hole had no effect on the net failure strength, indicating that off-axis specimens are less sensitive to the circular holes. To explain the influence of the extent of damage propagation mechanisms on notch sensitivity, Fig. 3(f) shows the comparison of theoretical failure initiation load based on net-SCF and gross-SCF (summarised in Table 6) with experimental failure initiation load. The experimental failure initiation loads are significantly higher than the theoretically predicted failure initiation loads which are evaluated based on consideration of elastic stress concentration factors in orthotropic laminates. This highlights that both 3D-FRC are notched insensitive for damage initiation as well and it is not just the damage propagation mechanism which results in this insensitivity. In general, the notch insensitivity of FRC mainly depends on the modulus of elasticity and fracture toughness of polymer matrix, and fibre/matrix interface properties (Tankasala et al., 2018). The fracture toughness and failure strains of thermoplastic and thermoset matrices used in this study are 6% and 0.5 kJ/m^2, and 3.5% and 0.12 kJ/m^2, respectively (Shah et al., 2021b). This indicates that the thermoplastic matrix exhibits up to 72% higher failure strain and 3 times higher fracture toughness. Additionally, Elium® provides better interface properties with E-glass fibres compared to epoxy resin (Shah et al., 2021d). Thus, higher failure strains, fracture toughness and better interface properties delay the propagation of cracks in the presence of the notches and make these composites notch insensitive.

It must be emphasized, however, that the above discussion about the notch insensitivity of both 3D-FRC is limited in terms of generality because of the well-known size effect observed in both 2D and 3D-FRC. The size effect is an important factor in determining FRC's notched response. In general, increasing the size of specimens with a constant diameter-to-width ratio decreases the strength of FRC (Mohammadi et al., 2017). Bazant et al. (Awerbuch and Madhukar, 1985) studied the size effect in edge-notched composites and proposed a size effect law to determine the nominal strength of unidirectional composites. The authors found that as the size of geometrically scaled composite increases, it exhibits a smooth ductile to brittle transition. Marco et al. (Yudhanto et al., 2012) used the size effect law to predict the interlaminar fracture energy of textile composites using single-edge notched specimens. Recently, Weixin et al. (Dai et al., 2015) used the size effect law to predict the interlaminar fracture toughness of 3D textile composites for the first time. While these studies are important in their own right, the authors in the current study focused on the differences in the behaviour of thermoset and thermoplastic 3D-FRC and did not attempt to account for the size effect for these cases, which can be investigated in a separate study. Besides the structural size effect, there may also be a material size

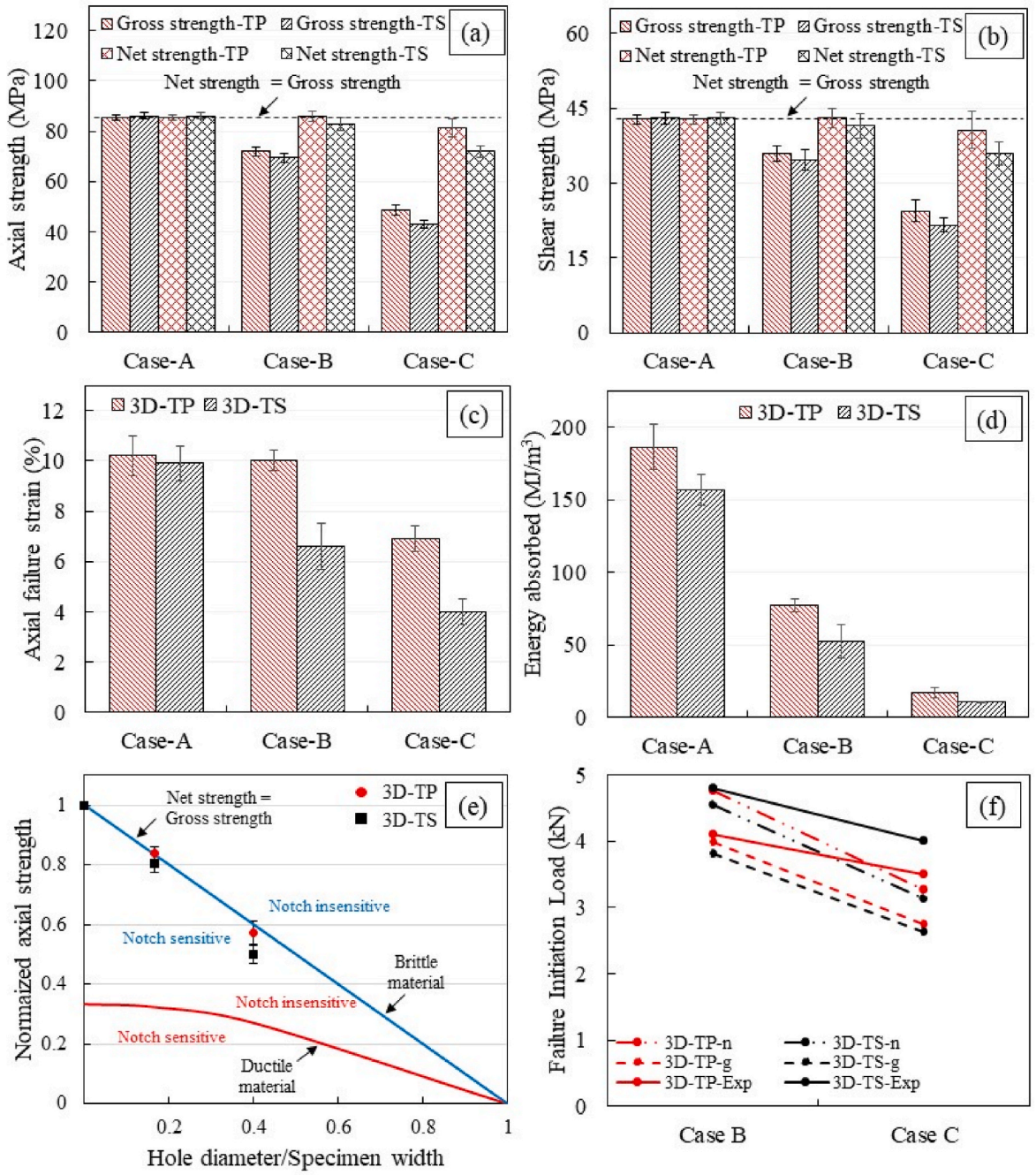

Fig. 3. Comparison of strength, failure strains and notched sensitivity of 3D-FRC. (a) Comparison of gross and net strength, (b) comparison of the net and gross shear strength, (c) comparisons of notched/unnotched localized failure strains, (d) energy absorbed in each case, (e) normalized strength vs. hole diameter/specimen width and (f) comparison of theoretical failure initiation load based on net-SCF and gross-SCF with experimental failure initiation load.

Table 6
Stress concentration factor and load reduction.

Stress concentration factor (SCF)				Theoretical failure initiation load (kN)			Exp. failure initiation load (kN)		
		Case-B	Case-C		Case-B	Case-C		Case-B	Case-C
K_{tn}	*3D-TP*	1.50	1.56	$F_{TP,n}^{ini}$	4.75	3.25	F_{TP}^{ini}	4.1	3.5
	3D-TS	1.58	1.64	$F_{TS,n}^{ini}$	4.53	3.12	F_{TP}^{ini}	4.8	4.0
K_{tg}	*3D-TP*	1.79	1.87	$F_{TP,g}^{ini}$	3.96	2.72			
	3D-TS	1.89	1.96	$F_{TS,g}^{ini}$	3.80	2.62			

effect in textile composites if the representative unit cell size of the composite is equal to or larger than the size of the ligament. In our case, the unit cell size of the 3D orthogonal fabric used is 2.1 mm × 2.85 mm x 0.46 mm. This indicates that the ligament covers almost 4-unit cells in Case-B and 3-unit cells in Case-C. Thus, we will not expect a significant material size effect in this case. However, the structural size effect may still be present as discussed earlier, and therefore the data reported in this study should be seen in the light of these limitations. Furthermore it should be noted that while the exact values are expected to change due to size effect, this change is expected to have similar trend in both these types of composites as the reinforcement architecture is same and thus the overall conclusions drawn about the influence of the two different matrix types, will still remain valid.

3.2. Comparison of strain field and failure mechanisms

Fig. 4 shows the comparison of strain fields (tensile strain along the y-axis ε_y) among notched and unnotched 3D-FRC at different axial strains, obtained from DIC. The unnotched specimens show almost similar failure strains (~10%), this suggests that the final failure is due to significant rotating of yarns. In Fig. 4(a), for un-notched thermoplastic 3D-FRC, a 45° fringe-like strain pattern can be seen throughout the specimen for higher strains (6% and higher) whereas for thermosets this fringe seems to be concentrated near the middle of the specimens. The more diffused pattern emerges as the thermoplastic matrix plastically deforms while still allowing for fibres to take most of the load. In contrast, the thermoset matrix develops cracks along the 45° shear plane much earlier on in the deformation process. These are identified as the highest strained fringe near the middle for strains greater than 2% (Fig. 4). These differences in failure mechanisms result in greater notch sensitivity and higher failure strains of the thermoplastic 3D-FRC. The notched specimens clearly elucidate this difference in strain pattern which is a consequence of the differences in the ductility of the polymer matrix as well as their fracture toughness. The thermoplastic 3D-FRC specimens due to their higher failure strains and fracture toughness failed after significant axial strain compared to thermoset 3D-FRC (see Fig. 4(b) and (c)). This higher strain to failure and ductility decreases stress-concentration at the hole periphery, redistributes stresses away from the hole and delays the propagation of cracks, which makes these composites more notch insensitive. In contrast, brittle epoxy matrix and lower fracture toughness facilitate propagation of cracks at a lower strain value, which accrue sudden failure.

A more detailed comparison of strain field development for the 0.164 diameter-to-width ratio specimen is shown in Fig. 5. The stress/strain curves of off-axis notched thermoplastic and thermoset 3D-FRC (Case-B). The strains in Fig. 5 (a) and (b) represents global axial strain along

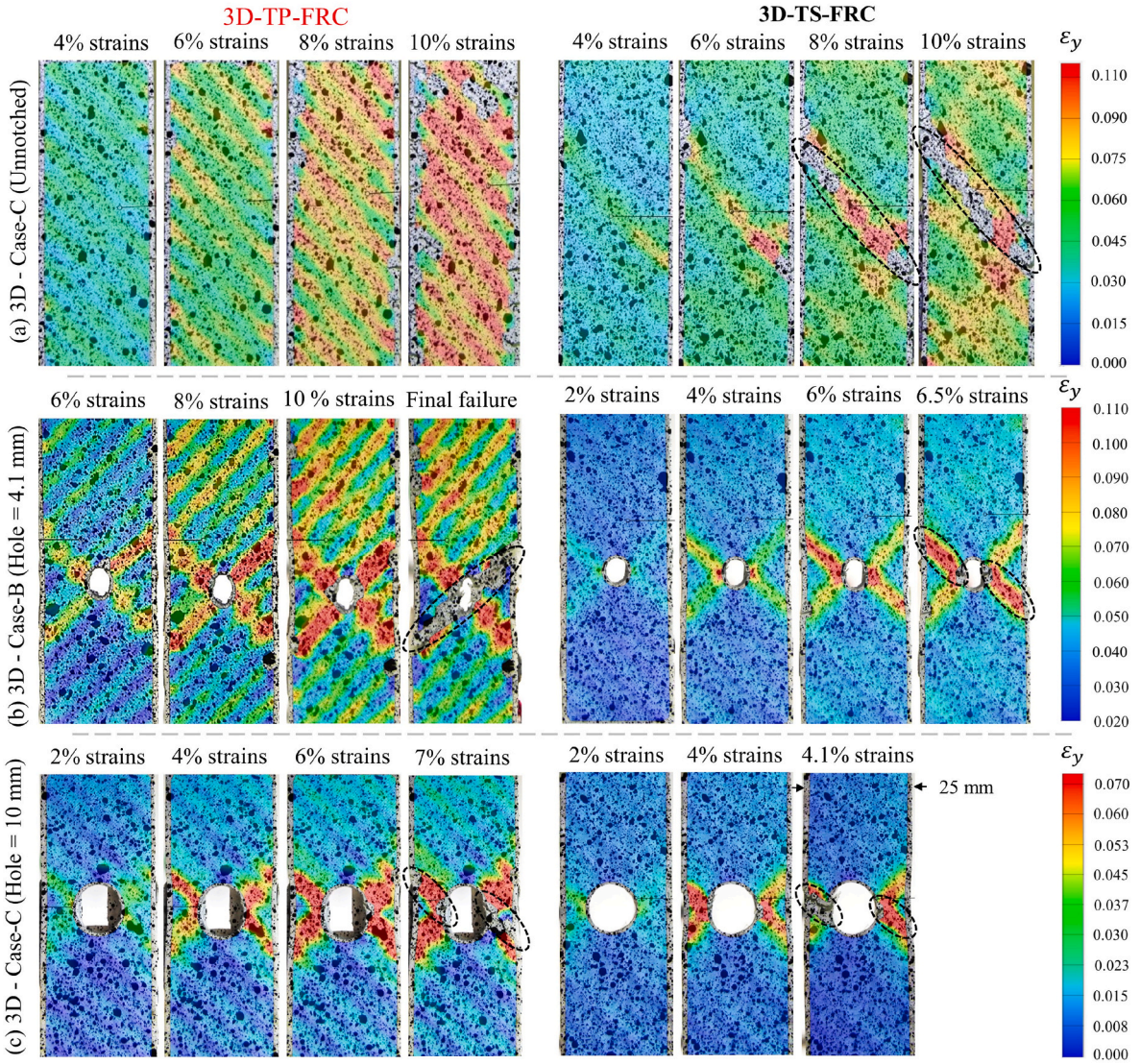

Fig. 4. Strain field in open-hole and unhole specimens obtained from DIC. (a) Case-A, (b) Case-B and (c) Case-C.

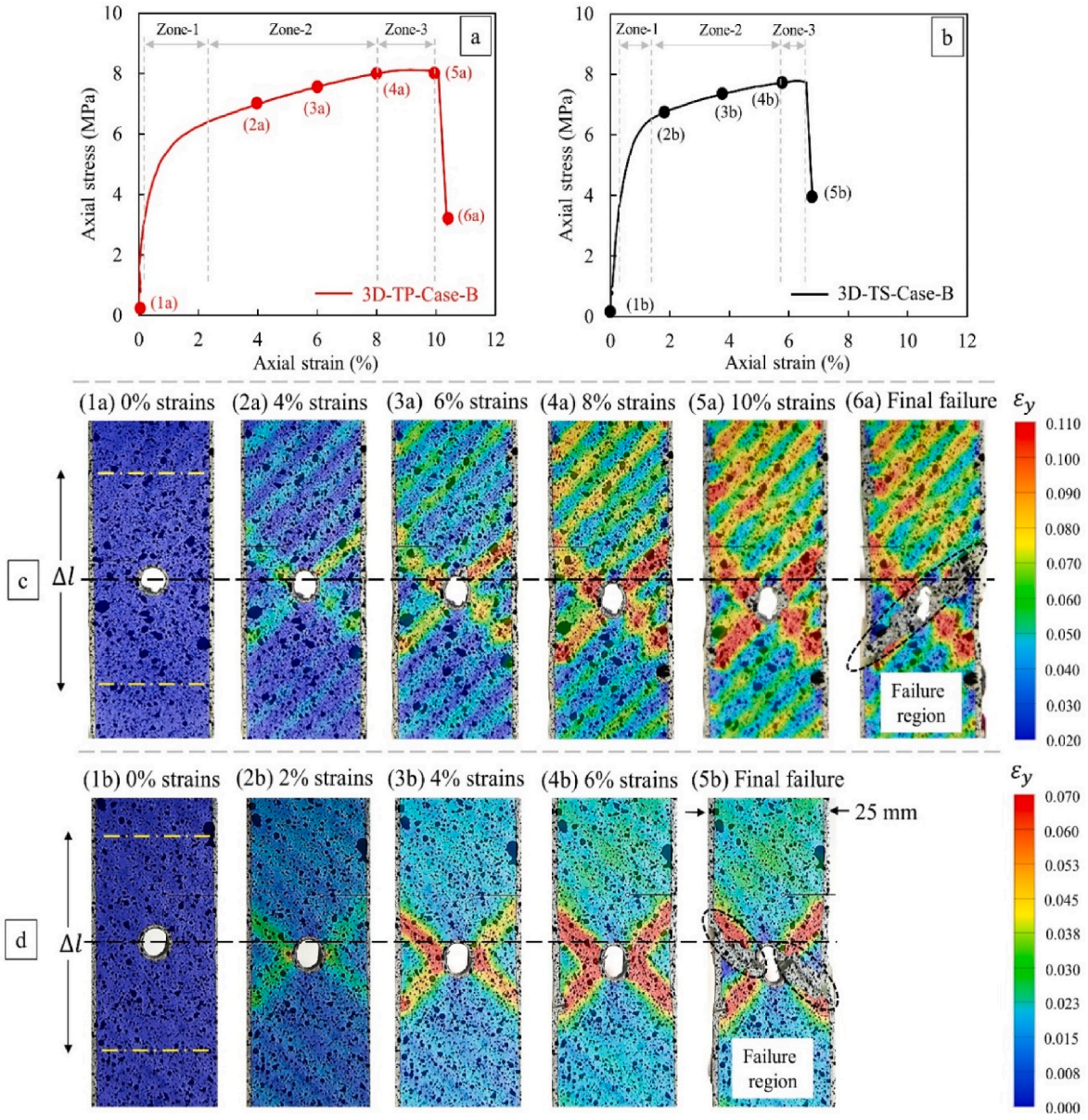

Figure 5. Strain distribution in each case obtained from DIC. (a) Case-A, (b) Case-B and (c) Case-C.

the width of the specimen. The axial strains increase linearly with axial stress up to the elastic limit, this is followed by the three main zones highlighted in the stress/strain curves of both 3D-FRC. The *"zone-1"* begins with the transition from the linear-to-nonlinear region. The nonlinear deformation in this zone is strongly influenced by the matrix properties. Due to the higher ductility and fracture toughness of thermoplastic 3D-FRC, they exhibit up to 66% higher nonlinear shear deformation (i.e., 2.5% axial strains) and show a rapid decrease in the tensile modulus, compared to thermoset 3D-FRC. The nonlinear deformation is followed by the linear region, i.e., *"zone-2"*. In this zone, axial strain increases linearly, due to the rotation of yarns/fibres which carry most of the axial load. The rotation of yarns also called the scissoring effect, allows the specimen to undergo large deformation. During this phase, the load increases linearly due to large matrix deformation and progressive rotation of yarns (stage (2a) to (5a) in Fig. 5(c) and stage (2 b) to (4 b) in Fig. 5(d)). In *"zone-3"*, the load-carrying capacity of the material decreases, resulting in the abrupt failure at ~45° (stage (6a) in Fig. 5(c) and stage (5 b) in Fig. 5(d)). The notched thermoplastic 3D-FRC specimens (Case-B) depict almost similar failure strains compared to unnotched specimens (Case-A), in contrast, notched thermoset 3D-FRC specimens show up to 33% less failure strains than the unnotched case.

Fig. 5 Strain distribution in 3D-FRC Case-B obtained from DIC. (a) Axial stress/strain curve of thermoplastic 3D-FRC, (b) axial stress/strain curve of thermoset 3D-FRC, (c) strains distribution in thermoplastic 3D-FRC, and (d) strains distribution in thermoset 3D-FRC. Δl represents strain measurement location 50 mm apart.

4. Conclusion

This study presents off-axis notched (Case-A) and unnotched (Case-B and Case-C) performance of resin-infused thermoplastic 3D-FRC under axial tensile loads. The ultimate strength, failure strains and strain field distribution obtained from 2D-DIC were evaluated and compared with conventional thermoset 3D-FRC. The unnotched 3D-FRC showed almost similar peak load and failure strains (~10%), due to significant rotation of yarns (Case-A). Among notched specimens, thermoplastic 3D-FRC (Case-B) depicts an almost similar failure strain, as observed in Case-A. In contrast, thermoset 3D-FRC showed up to 33% (Case-B) and 60% (Case-C) reduction in the failure strains, compared to thermoset 3D-FRC. Among 3D-FRC, thermoplastic 3D-FRC presented notch insensitivity and

higher energy absorption for both cases (Case-B and Case-C) for the specimen geometry investigated, indicating that the thermoplastic resin has improved damage tolerance in a comparative sense. The notch insensitivity of thermoplastic 3D-FRC is primarily due to higher ductility, fracture toughness of the polymer matrix, as well as superior fibre/matrix interface properties. This study elucidates that for FRC joints, off-axis resin-infused thermoplastic 3D-FRC exhibits potential for overcoming the current challenges faced by composite laminates. The strengths, failure strains and extent of notch insensitivity reported in this work are meaningful only for the geometry and the cases investigated due to the influence of size effect in OHT tests and this will be investigated in a further study. In a relative sense however the results indicate thermoplastic 3D-FRC to be more notch insensitive than the thermoset counterpart.

Declaration of competing interest

The authors declare that they have no known competing financial interests or personal relationships that could have appeared to influence the work reported in this paper.

Data availability

Data will be made available on request.

Acknowledgements

The authors would like to acknowledge the financial support provided by Universiti Teknologi PETRONAS (Grant number 015LA0-031). The author would also like to acknowledge the support of Sharp Keith from Textech industries for providing the 3D fabric for this research work. The authors are grateful to Barsotti Robert and Pierre Gerard from Arkema for providing Elium® resin for this research work.

References

Ahmed, T., Choudhry, R., Ullah, H., Hassan, F., 2015. Numerical modelling of carbon fibre reinforced polymer composites for hole size effect. NUST Journal of Engineering Sciences 8 (1), 1–9.

ASTM, 2017. D3039/D3039M-17 Standard Test Method for Tensile Properties of Polymer Matrix Composite Materials.

ASTM D5766/D5766M-11(2018), 2018. Standard Test Method for Open-Hole Tensile Strength of Polymer Matrix Composite Laminates. ASTM International, West Conshohocken, PA. www.astm.org.

Awerbuch, J., Madhukar, M.S., 1985. Notched strength of composite laminates: predictions and experiments. A review. J. Reinforc. Plast. Compos. 4 (1), 3–159.

Bhudolia, S.K., Perrotey, P., Joshi, S.C., 2017. Optimizing polymer infusion process for thin ply textile composites with novel matrix system. Materials 10 (3), 293.

Dai, S., Cunningham, P.R., Marshall, S., Silva, C., 2015. Open hole quasi-static and fatigue characterisation of 3D woven composites. Compos. Struct. 131, 765–774.

Guo, Q., Zhang, Y., Li, D., Li, M., Sun, X., Chen, L., 2021. Tensile properties and failure mechanism of 3D woven composites containing holes of different geometries. Thin-Walled Struct. 166, 108115.

Hodgkinson, J., 2012. Testing the Strength and Stiffness of Polymer Matrix Composites. Failure Mechanisms in Polymer Matrix Composites. Elsevier, pp. 129–182.

Kazemi, M.E., Shanmugam, L., Lu, D., Wang, X., Wang, B., Yang, J., 2019. Mechanical properties and failure modes of hybrid fiber reinforced polymer composites with a novel liquid thermoplastic resin. Elium®. Composites Part A: Applied Science and Manufacturing 125, 105523.

Mohammadi, R., Najafabadi, M.A., Saeedifar, M., Yousefi, J., Minak, G., 2017. Correlation of acoustic emission with finite element predicted damages in open-hole tensile laminated composites. Compos. B Eng. 108, 427–435.

Muñoz, R., Martínez, V., Sket, F., González, C., Llorca, J., 2014. Mechanical behavior and failure micromechanisms of hybrid 3D woven composites in tension. Compos. Appl. Sci. Manuf. 59, 93–104.

Russo, A., Zuccarello, B., 2007. An accurate method to predict the stress concentration in composite laminates with a circular hole under tensile loading. Mech. Compos. Mater. 43 (4), 359–376.

Sajid, Z., Karuppanan, S., Kee, K.E., Sallih, N., Shah, S.Z.H., 2021a. Carbon/basalt hybrid composite bolted joint for improved bearing performance and cost efficiency. Compos. Struct. 275, 114427.

Sajid, Z., Karuppanan, S., Sallih, N., Kee, K.E., Shah, S.Z.H., 2021b. Role of washer size in mitigating adverse effects of bolt-hole clearance in a single-lap, single-bolt basalt composite joint. Compos. Struct. 266, 113802.

Sajid, Z., Karuppanan, S., Kee, K.E., Sallih, N., Shah, S.Z.H., 2022. Bearing performance improvement of single-lap, single-bolt basalt composite joints by locally strengthening the joint location using carbon fibre. Thin-Walled Struct. 180, 109873.

Saleh, M.N., Wang, Y., Yudhanto, A., Joesbury, A., Potluri, P., Lubineau, G., et al., 2016. Investigating the potential of using off-Axis 3D woven composites in composite joints' applications. Appl. Compos. Mater. 24 (2), 377–396.

Shah, S.Z.H., Choudhry, R.S., Khan, L.A., 2017. Challenges in compression testing of 3D angle-interlocked woven-glass fabric-reinforced polymeric composites. ASTM Journal of Testing and Evaluation 5 (4), 1502–1523.

Shah, S.Z.H., Karuppanan, S., Megat-Yusoff, P., Sajid, Z., 2019. Impact resistance and damage tolerance of fiber reinforced composites: a review. Compos. Struct. 217, 100–121.

Shah, S.Z.H., Megat-Yusoff, P., Karuppanan, S., Choudhry, R., Ahmad, F., Sajid, Z., et al., 2020. Performance comparison of resin-infused thermoplastic and thermoset 3D fabric composites under impact loading. Int. J. Mech. Sci. 189, 105984.

Shah, S.Z.H., Megat-Yusoff, P., Karuppanan, S., Choudhry, R., Sajid, Z., 2021a. Multiscale damage modelling of 3D woven composites under static and impact loads. Compos. Appl. Sci. Manuf. 151, 106659.

Shah, S.Z.H., Megat-Yusoff, P., Karuppanan, S., Choudhry, R., Ud Din, I., Othman, A., et al., 2021b. Compression and buckling after impact response of resin-infused thermoplastic and thermoset 3D woven composites. Compos. B Eng. 207, 108592.

Shah, S.Z.H., Megat-Yusoff, P.S.M., Choudhry, R.S., Sajid, Z., Din, I.U., 2021c. Experimental investigation on the quasi-static crush performance of resin-infused thermoplastic 3D fibre-reinforced composites. Compos. Commun. 28, 100916.

Shah SZH, Megat-Yusoff PSM, Karuppanan S, Choudhry RS, Ahmad F, Sajid Z. Mechanical properties and failure mechanisms of novel resin-infused thermoplastic and conventional thermoset 3D fabric composites. Appl. Compos. Mater.. 2021(29): 515–545.

Shah, S.Z.H., Megat-Yusoff, P.S.M., Karuppanan, S., Choudhry, R.S., Sajid, Z., 2022. Off-Axis and on-Axis performance of novel acrylic thermoplastic (Elium®) 3D fibre-reinforced composites under flexure load. Polymers 14 (11).

Song, J., Wen, W., Cui, H., Wang, Y., Lu, Y., Long, W., et al., 2019. Warp direction fatigue behavior and damage mechanisms of centrally notched 2.5D woven composites at room and elevated temperatures. Compos. Sci. Technol. 182, 107769.

Tan, S.C., 1988. Finite-width correction factors for anisotropic plate containing a central opening. J. Compos. Mater. 22 (11), 1080–1097.

Tankasala, H.C., Deshpande, V.S., Fleck, N.A., 2018. Notch sensitivity of orthotropic solids: interaction of tensile and shear damage zones. Int. J. Fract. 212 (2), 123–142.

Yudhanto, A., Watanabe, N., Iwahori, Y., Hoshi, H., 2012. The effects of stitch orientation on the tensile and open hole tension properties of carbon/epoxy plain weave laminates. Mater. Des. 35, 563–571.

Zhang, H., Yang, J., 2014. Development of self-healing polymers via amine–epoxy chemistry: II. Systematic evaluation of self-healing performance. Smart Mater. Struct. 23 (6).